Journal of Alloys and Compounds 372 (2004) 148–157

Journal of ALLOYS AND COMPOUNDS

www.elsevier.com/locate/jallcom

The interfacial reactions of infrared brazing Cu and Ti with two silver-based braze alloys

R.K. Shiue [a], S.K. Wu [b,*], C.H. Chan [b]

[a] *Department of Materials Science and Engineering, National Dong Hwa University, Hualien 974, Taiwan*
[b] *Department of Materials Science and Engineering, National Taiwan University, Taipei 106, Taiwan*

Received 18 August 2003; received in revised form 30 September 2003; accepted 30 September 2003

Abstract

The microstructural evolution and shear strength of the infrared brazed Cu and Ti with two silver-based braze alloys are studied. The dissolution between the molten braze and Cu substrate is much more prominent than that of Ti substrate. For specimens infrared brazed with pure Ag, the molten braze is separated into Ag-, Cu- and Ti-rich liquids. The Ag-rich liquid overflows out of the joint, so only the liquid rich in Cu and Ti is left in the joint. The joint is primarily comprised of Cu_4Ti and Cu_2Ti phases, and three interfacial reaction layers, $CuTi_2$, CuTi and Cu_4Ti_3 are observed after infrared brazing. For specimens infrared brazed with 72Ag–28Cu, the microstructural evolution is well elucidated by the Ag–Cu–Ti ternary alloy phase diagram, and its shear strength is strongly related to the presence of interfacial phases between Ti and the braze alloy.

Keywords: Bonding; Silver-based braze alloys; Titanium and copper; Microstructure; Mechanical properties

1. Introduction

Infrared brazing makes use of infrared energy generated by heating a tungsten filament in quartz tube as the heating source, providing a rapid heating rate up to 3000 °C/min [1–5]. Additionally, the infrared rays can easily transmit through the quartz tube, and not be absorbed by the quartz furnace itself. Using an appropriate optical focusing system, locally heating of the joint can be obtained. Therefore, infrared brazing is featured with both high-speed thermal cycles and high-energy efficiency, making it a very promising technique among all joining processes [3].

A fast brazing thermal cycle is important for certain applications in order to avoid liquation of the molten braze [6]. For the brazing filler metal with different solidus and liquidus temperatures, the composition of the melt changes gradually as the temperature increases from the solidus to liquidus. If the portion that melts first is allowed to flow out, the remaining solid may not melt and may remain behind as a residue, which is called liquation [6]. Filler metal with a wide melting range needs rapid heating cycles to minimize separation during brazing. Therefore, a fast thermal cycle is crucial for certain braze alloys with wide melting ranges. Additionally, it is also noted that most interfacial reactions between the base metal and braze alloy can be inhibited or slowed down by using a rapid brazing thermal cycle [7,8].

The bonding between pure titanium and copper is encountered in production of the titanium target used in the physical vapor deposition (PVD) facility. The titanium target is joined with the water-cooled oxygen-free copper substrate. There are many joining processes available in bonding dissimilar alloys. For example, pure Ti and Cu can be bonded using adhesive bonding, mechanical fastening, friction welding and brazing, etc. [8,9]. Brazing is probably one of the best choices in this case due to high thermal conductivity of the brazed joint. It has been reported that titanium and its alloys can be brazed with silver-based braze alloys [6–11]. Although the TiAg intermetallic compound is formed in brazing Ti alloys using pure silver as the filler metal, TiAg is not as brittle as most of other intermetallics [7,10,11]. There is no elongation and/or ductility data available for TiAg intermetallic compound in the literature. The ductile nature of the TiAg intermetallic compound is demonstrated by the existence of dimples on its fractured surface

* Corresponding author. Tel.: +886-2-2363-7846; fax: +886-2-2363-4562.
E-mail address: skw@ccms.ntu.edu.tw (S.K. Wu).

0925-8388/$ – see front matter © 2003 Elsevier B.V. All rights reserved.
doi:10.1016/j.jallcom.2003.09.155

Table 1
The silver-based braze alloys used in the experiment

Alloy	Nominal composition (wt.%)	Solidus/liquidus (°C)
Ag	100Ag	961/961
BAg-8	72Ag–28Cu	780/780

[11]. In contrast, fractographs of many other intermetallics, e.g. TiCu, $TiAl_3$ and TiFe, etc. are usually dominated by cleavage fracture. Therefore, most Ti alloys brazed by the silver-based filler metal demonstrate good bonding strength [3,8–12]. Additionally, pure copper is also readily brazed using the silver-based braze alloy [6,8,9]. Consequently, the pure silver is selected as the brazing filler metal in the study. In addition to the pure silver, 72Ag–28Cu in weight percent featured with a much lower melting temperature of 780 °C is also used as the filler metal in brazing Cu and Ti. The purpose of this investigation is to study the infrared brazing of Ti and Cu substrates using two silver-based braze alloys. Both the microstructural evolution and bonding strength of the infrared brazed joint are extensively evaluated.

2. Experimental procedures

The base metals used in the experiment were the commercially pure titanium plate (CPTi) in the form of 10 mm × 10 mm × 2 mm and the oxygen-free copper plate with the dimension of 10 mm × 15 mm × 5 mm, respectively. The nominal composition of the commercially pure titanium in weight percent is 0.08% C, 0.20% Fe, 0.03% N, 0.18% O, 0.015% H and balance Ti. The chemical composition of the oxygen-free copper in weight percent is 99.95% Cu and 0.003% P. The base metals were first polished with SiC papers and subsequently cleaned by an ultrasonic bath using acetone as the solvent prior to infrared brazing. There were two silver-based braze alloys available in the experiment, including pure Ag and 72Ag–28Cu (wt.%). Based on the AWS specification for silver-based braze alloys, the chemical composition of 72Ag–28Cu alloy was in accordance with the BAg-8 braze alloy [6,8]. Table 1 illustrates the chemical compositions, solidus and liquidus temperatures of these silver-based braze alloys. Additionally, braze alloy foils with the thickness of 100 μm were applied throughout the experiment.

Infrared brazing was performed in a vacuum of 8×10^{-5} mbar, and the heating rate was set at 900 °C/min throughout the experiment. To enhance the absorption of infrared rays, a graphite fixture was used during brazing as described in the previous studies [1,3–5]. Specimens were sandwiched between two graphite plates, and an R-type thermal couple was inserted into the upper graphite plate, in contact with the brazed specimen. The area of filler metal foil was approximately the same as that of base metal. All specimens were preheated to 500 °C for 90 s before they were heated up to the brazing temperature. Because there was a time delay between the actual specimen temperature and programmer temperature, time compensation was included throughout the experiment [3–5]. The brazing time specified in the test was the actual specimen holding time. Table 2 summarized all infrared brazing process variables used in bonding copper and titanium.

Table 2
The process variables used in the infrared brazing

Filler metal	Time (s)	800 °C	850 °C	980 °C	1000 °C
Ag	30			M	M
	60			M	M
72Ag–28Cu	30	M/S	M/S		
	60	M/S	M/S		

M: metallographic observation specimen; S: shear test specimen.

The infrared brazed specimens were cut by a low speed diamond saw, followed by experiencing a standard metallographic procedure. 2 g CrO_3 + 2 ml H_2SO_4 + 1000 ml water was used as the etching solution prior to metallographic examination. The cross-section of the brazed specimens was examined using either LEO 1530 field emission scanning electron microscope (FESEM) or Philips XL-30 scanning electron microscope (SEM) with an accelerating voltage of 15 kV. Quantitative chemical analyses were performed using a JEOL JXL-8600SX electron probe microanalyzer (EPMA) with an operation voltage of 20 kV and spot size of 1 μm. The intensities of Cu Kα, Ti Kα and Ag Lα characteristic lines were measured for the EPMA analyses. Additionally, pure Ag, Cu and Ti were used as the standards, respectively.

The shear test was performed to evaluate the bonding strength of the infrared brazed specimen. Fig. 1 displays the schematic diagram of the specimen used in the shear test. The shaded areas in the graph were Cu and Ti substrates, and the outer part of the layout was the graphite fixture used in the infrared brazing [3–5]. Two bold lines with the width of 1.5 mm in the figure illustrated the location of the braze alloy. The brazed specimen was compressed by a Shimadzu AG-10 universal testing machine with a constant speed of 1 mm/min. The fractured surface after shear test was firstly examined by an SEM, and followed by a structural analysis. The structure analysis was performed using a Philips PW1710 X-ray diffractometer. Cu Kα was selected as the X-ray source. The X-ray scan rate was set at 4°/min, and its range was between 30° and 80°.

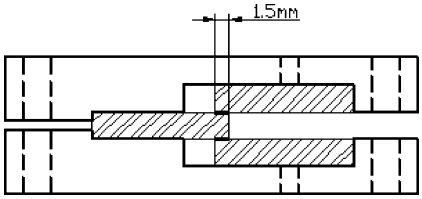

Fig. 1. The schematic diagram of the specimen used in the shear test.

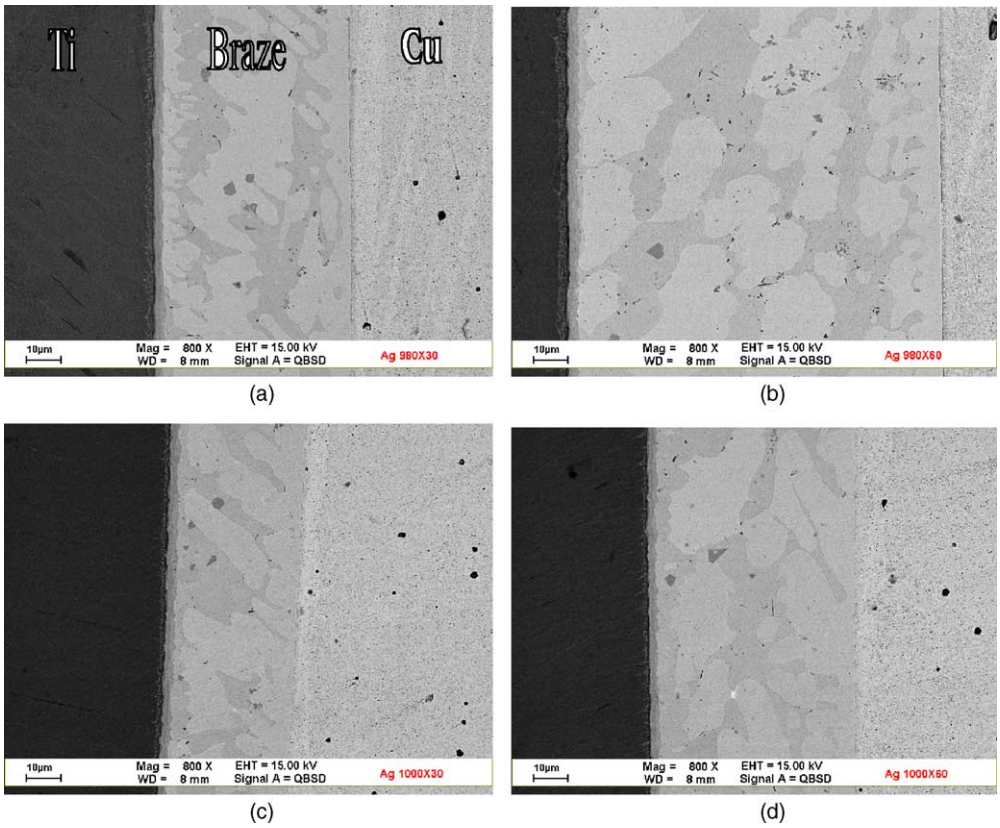

Fig. 2. The SEM BEIs of Ti/Ag/Cu specimens infrared brazed at (a) 980 °C × 30 s, (b) 980 °C × 60 s, (c) 1000 °C × 30 s, (d) 1000 °C × 60 s.

3. Results and discussion

3.1. Infrared brazing of Ti and Cu using pure silver

Fig. 2 shows the SEM backscattered electron images (BEIs) of Ti/Ag/Cu infrared brazed joints for various brazing conditions. The backscattered image does not provide topographic contrast but primarily shows the element distribution in the brazed joint [7,13]. According to Fig. 2, both Ti and Cu substrates were dissolved into the molten braze during brazing, and the dissolution of substrates into the molten braze resulted in the chemical composition of the braze alloy deviating from pure silver. Additionally, the dissolution between molten braze and Cu substrate was much more prominent than that of Ti substrate. Fig. 3 shows the SEM BEI and EPMA chemical analysis results of Ti/Ag/Cu specimen infrared brazed at 980 °C for 30 s. The EPMA analysis at point B in Fig. 3 is not a reliable data due to its thickness much lower than 1 μm. In contrast, the accuracy of points C and D is much better than that of point B, because the width of reaction layer at point C and D is about 1 μm. Based on the EPMA chemical analysis, the brazed joint is primarily comprised of Cu_4Ti (marked by E) and Cu_2Ti (marked by F). There are at least two interfacial phases, including: CuTi (marked by C) and Cu_4Ti_3 (marked by D) as shown in Fig. 3. It is also important to note that the silver content in the brazed joint is almost disappeared.

The Ag-rich liquid was formed as the brazing temperature increased above its melting point. Both Ti and Cu substrates were dissolved into the molten braze during infrared brazing. Fig. 4 shows the liquidus projection of Ag–Cu–Ti ternary alloy phase diagram, and the important reaction scheme is also included [14]. The achievement of equilibrium in solid-state transformation is always a major concern in application of the phase diagram, and the existence of actual phase(s) could be far way from the equilibrium phase diagram. However, the concern is greatly decreased for the solid–liquid transformation. The mass transport is highly enhanced in the solid–liquid transformation as compared with that in the solid-state transformation. There are at least three major metallurgical phenomena during infrared brazing, including: melting of the braze alloy, dissolution of the substrate(s) and solidification of the molten braze. All above metallurgical phenomena involve solid–liquid transformation. Consequently, the equilibrium Ag–Cu–Ti ternary alloy phase diagram is cited in the study. According to the Fig. 4, there is a huge miscibility gap among the liquids. The molten braze tends to separate into two liquids. One is rich in Ag, and the other is rich in both Cu and Ti. For instance, two immiscible liquids, L_1 and L_2, at 982 °C, and its reaction scheme is illustrated below [14]:

$$L_1 + (Ti)(HT) \leftrightarrow L_2 + CuTi_2 \quad (982\,^{\circ}C) \tag{1}$$

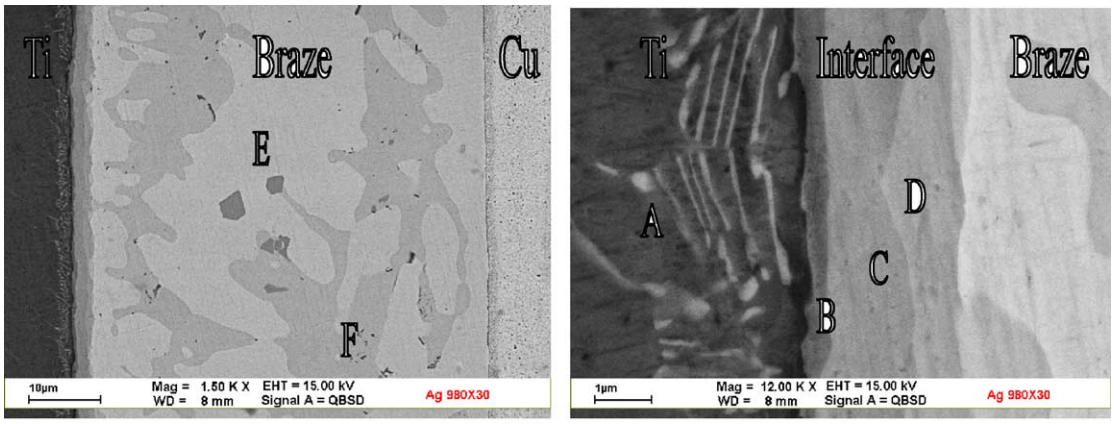

at%	A	B	C	D	E	F
Ag	0.5	0.0	0.0	0.4	0.2	0.3
Cu	12.2	35.7	50.3	56.7	76.4	67.1
Ti	87.3	64.3	49.7	42.9	23.4	32.6
Phase	Ti-rich ($CuTi_2$)		CuTi	Cu_4Ti_3	Cu_4Ti	Cu_2Ti

Fig. 3. The SEM BEIs and EPMA chemical analysis results of Ti/Ag/Cu specimen infrared brazed at 980 °C for 30 s.

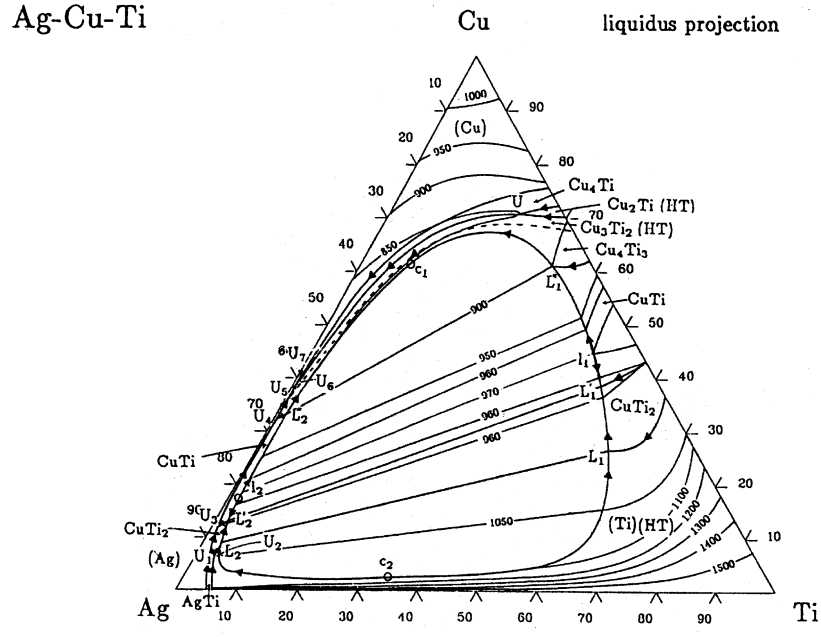

	$l_1 \rightleftharpoons l_2 + CuTi$	970°C
c_1:	$l \rightleftharpoons Cu_4Ti_3$	~ 850°C l = 30 at.% Ag , 61 at.% Cu
c_2:	$l \rightleftharpoons (Ti)(HT)$	~ 1100°C l = 64 at.% Ag , 2 at.% Cu
	$L_1' \rightleftharpoons L_2' + CuTi + CuTi_2$	954°C
	$L_1 + (Ti)(HT) \rightleftharpoons L_2 + CuTi_2$	982°C
	$L_1'' + CuTi \rightleftharpoons L_2'' + Cu_4Ti_3$	900°C
U:	$L + Cu_2Ti(HT) \rightleftharpoons Cu_3Ti_2(HT) + Cu_4Ti$	851°C
U_1:	$L + (Ti)(HT) \rightleftharpoons AgTi + CuTi_2$	960°C
U_2:	$L + AgTi \rightleftharpoons (Ag) + CuTi_2$	929°C
U_3:	$L + CuTi_2 \rightleftharpoons (Ag) + CuTi$	908°C
U_4:	$L + CuTi \rightleftharpoons (Ag) + Cu_4Ti_3$	860°C
U_5:	$L + Cu_4Ti_3 \rightleftharpoons (Ag) + Cu_3Ti_2(HT)$	843°C
U_6:	$L + Cu_3Ti_2(HT) \rightleftharpoons (Ag) + Cu_4Ti$	808°C
U_7:	$L + Cu_4Ti \rightleftharpoons (Ag) + (Cu)$	783°C

Fig. 4. The liquidus projection of Ag–Cu–Ti ternary alloy phase diagram and its reaction scheme [14].

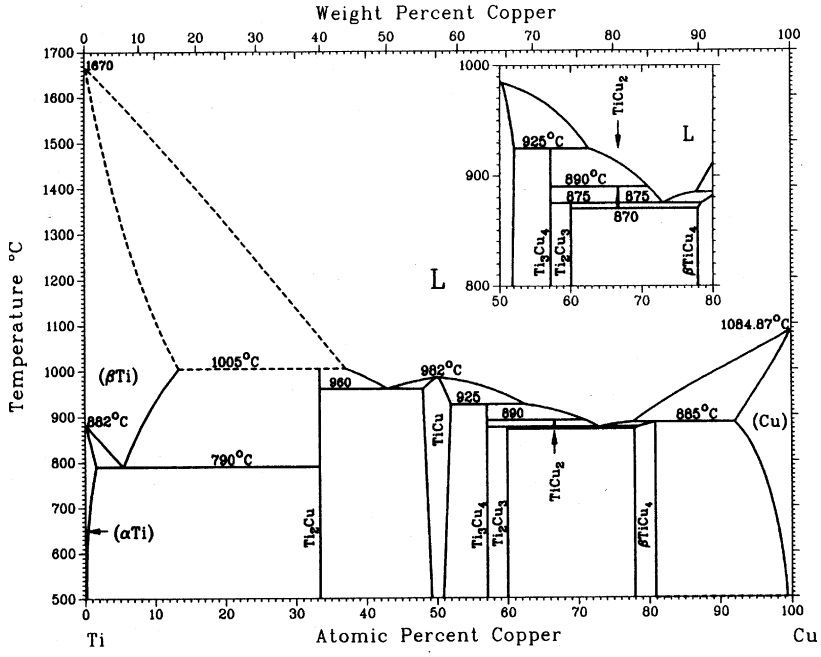

Fig. 5. The Cu–Ti binary alloy phase diagram [15].

The L_2 liquid is rich in Ag, and the L_1 liquid is rich in Cu and Ti. According to Fig. 3, the cooling path follows L_1 towards to L_1', and the reaction is shown below [14]:

$$L_1' \leftrightarrow L_2' + CuTi + CuTi_2 \quad (954\,^{\circ}C) \tag{2}$$

Similarly, the L_2' liquid is rich in Ag, and the L_1' liquid is rich in Cu and Ti. According to the experimental observation, both CuTi and $CuTi_2$ are found at the interface between the braze and Ti substrate as illustrated in Fig. 3, and it is consistent with Eqs. (1) and (2). Additionally, the Ag-rich liquids (L_2 and L_2') overflowed out of the joint, so only the liquid rich in Ti and Cu (L_1 and L_1') is left in the joint. Based on the liquidus projection of Ag–Cu–Ti ternary alloy phase diagram, the chemical composition of L_1' in atomic percent is 10Ag, 40Cu and 50Ti.

Because all phases in the brazed joint primarily consist of Ti and Cu as shown in Fig. 3, a Cu–Ti binary alloy phase diagram (Fig. 5) is cited here for convenience [15]. It is expected that the formation of interfacial CuTi and/or $CuTi_2$ phase results in isolation of the molten braze and Ti substrate for the specimen infrared brazed at 980 °C. Based on the Cu–Ti binary alloy phase diagram, a series of invariant reactions upon cooling of the liquid are listed below [15]:

$$CuTi + L \leftrightarrow Cu_4Ti_3 \quad (\text{peritectic},\ 925 \pm 10\,^{\circ}C) \tag{3}$$

$$Cu_4Ti_3 + L \leftrightarrow Cu_2Ti \quad (\text{peritectic},\ 890 \pm 10\,^{\circ}C) \tag{4}$$

$$L \leftrightarrow Cu_2Ti + \beta Cu_4Ti \quad (\text{eutectic},\ 875 \pm 10\,^{\circ}C) \tag{5}$$

If the solidification of molten braze follows the above Eqs. (3)–(5), the formation of interfacial Cu_4Ti_3 phase is caused by the peritectic reaction between the molten braze and CuTi phase. Accordingly, the interfacial Cu_4Ti_3 phase is subsequently reacted with the residual molten braze upon the cooling cycle, and the Cu_2Ti phase is formed via peritectic reaction. Finally, the residual molten braze is completely solidified into Cu_2Ti and Cu_4Ti via the eutectic reaction as shown in Eq. (5). The experimental result as demonstrated in Fig. 3 is consistent with the related phase diagrams.

The shear test of infrared brazed Ti/Ag/Cu joint could not be performed due to erosion of the Cu substrate. Fig. 6 illustrates the schematic diagrams of the shear test specimen before and after infrared brazing, respectively. The Ti plate is located at center of the shear test specimen, and two Cu plates are adjacent to the Ti plate. The copper substrates were severely dissolved into the molten braze during infrared brazing, so both Cu substrates were significantly eroded after infrared brazing. According to Fig. 6(b), shear strength of Cu and Ti substrates instead of the infrared brazed

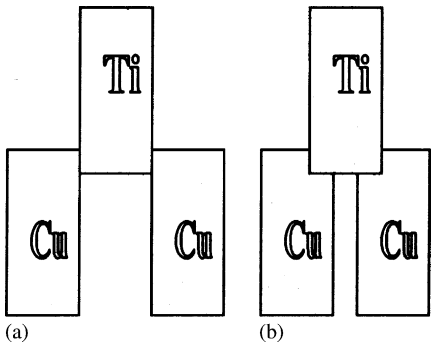

Fig. 6. The schematic diagrams of the shear test specimen (a) before infrared brazing and (b) after infrared brazing.

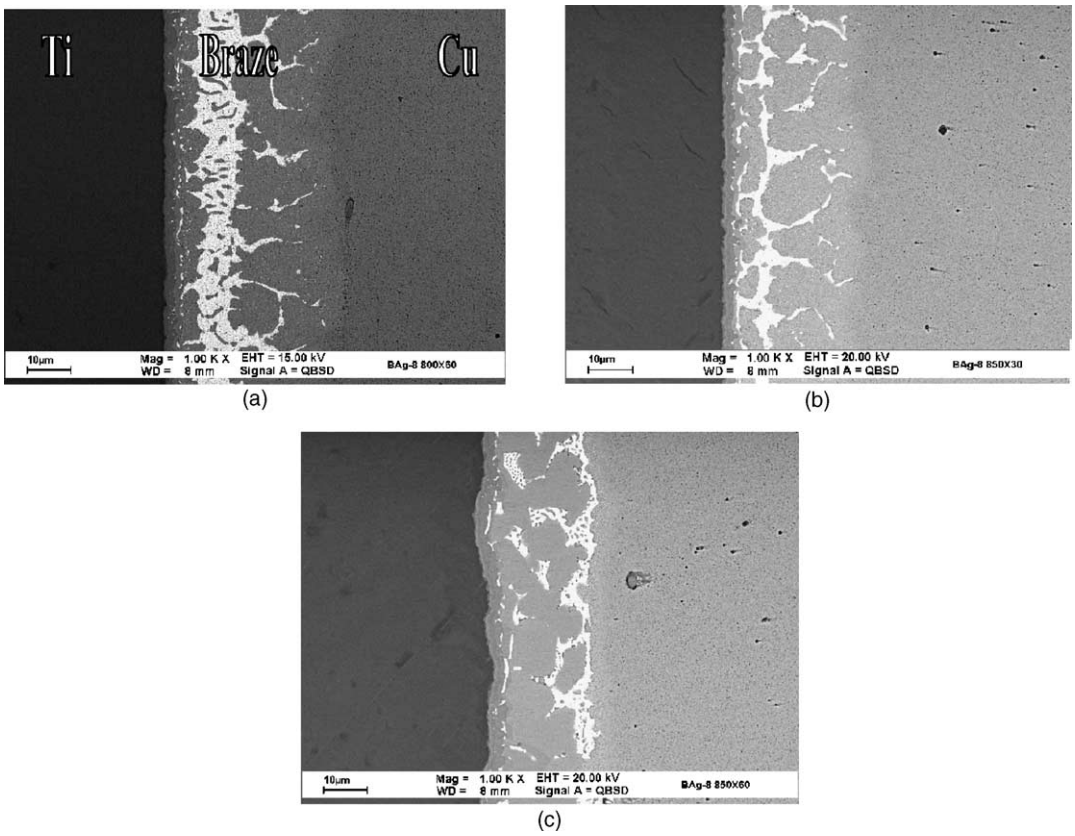

Fig. 7. The SEM BEIs of Ti/72Ag–28Cu/Cu specimens infrared brazed at (a) 800 °C × 60 s, (b) 850 °C × 30 s, (d) 850 °C × 60 s.

joint was measured in the shear test. Consequently, the shear strength of infrared brazed Cu/Ag/Ti joint could not be accurately determined in the experiment. Actually, the infrared brazed Ti/Ag/Cu specimen was not fractured even if the applied shear stress exceeded 400 MPa. Both Cu substrates were distorted if the applied shear stress exceeded 400 MPa. Consequently, there was no shear strength available for the Ti/Ag/Cu infrared brazed joint.

3.2. Infrared brazing of Ti and Cu using 72Ag–28Cu

Fig. 7 shows the SEM BEIs of Ti/72Ag–28Cu/Cu specimens infrared brazed at different brazing conditions. The microstructure of Ti/72Ag–28Cu/Cu joint is very different from that of Ti/Ag/Cu joint as compared between Fig. 2 and Fig. 7. Because the brazing temperature of 72Ag–28Cu braze is much lower than that of pure silver, overflow of the Ag-rich liquid during infrared brazing was greatly abated. Similar to the aforementioned result, the dissolution between molten braze and Cu substrate was much more prominent than that of Ti substrate. Additionally, there was no interfacial reaction between the braze and Cu substrate, but interfacial reaction layers were observed at the interface between Ti and braze.

Fig. 8 displays the SEM BEIs and EPMA chemical analysis results of Ti/72Ag–28Cu/Cu specimen infrared brazed at 850 °C for 60 s. The infrared brazed joint is primarily comprised of Cu_4Ti and Ag-rich phases, as marked by C and D in Fig. 8, respectively. At least two interfacial reaction layers are found in the figure. Based on the EPMA chemical analysis results, the stoichiometric ratios between Cu and Ti at the reaction layers are close to CuTi (marked by A) and Cu_4Ti_3 (marked by B). According to Fig. 4, the reaction at point c_1 is shown below [14]:

$$L \leftrightarrow Cu_4Ti_3(\sim 850\,^{\circ}C) \quad (6)$$

where the chemical composition in atomic percent of the liquid (L) is 30Ag, 61Cu and 9Ti. Based on the Eq. (6), Cu_4Ti_3 is readily formed from the molten braze with the chemical composition of 30Ag–61Cu–9Ti (at.%). Additionally, the interfacial Cu_4Ti_3 phase is also formed upon infrared brazing at 850 °C. There are several invariant reactions upon cooling of the infrared brazed specimen as shown below [14]:

$$U_5: \quad L + Cu_4Ti_3 \leftrightarrow (Ag) + Cu_3Ti_2(HT) \quad (843\,^{\circ}C) \quad (7)$$

$$U_6: \quad L + Cu_3Ti_2(HT) \leftrightarrow (Ag) + Cu_4Ti \quad (808\,^{\circ}C) \quad (8)$$

The interfacial Cu_4Ti_3 phase reacts with the molten braze upon cooling cycle, and both Ag-rich and Cu_3Ti_2(HT) phases are formed. The Cu_3Ti_2(HT) phase further reacts with the residual liquid and forms both Cu_4Ti and Ag-rich phases as illustrated in Eq. (8). According to the experimental observations, the residual molten braze is completely consumed at the transition reaction U_6. Consequently, the

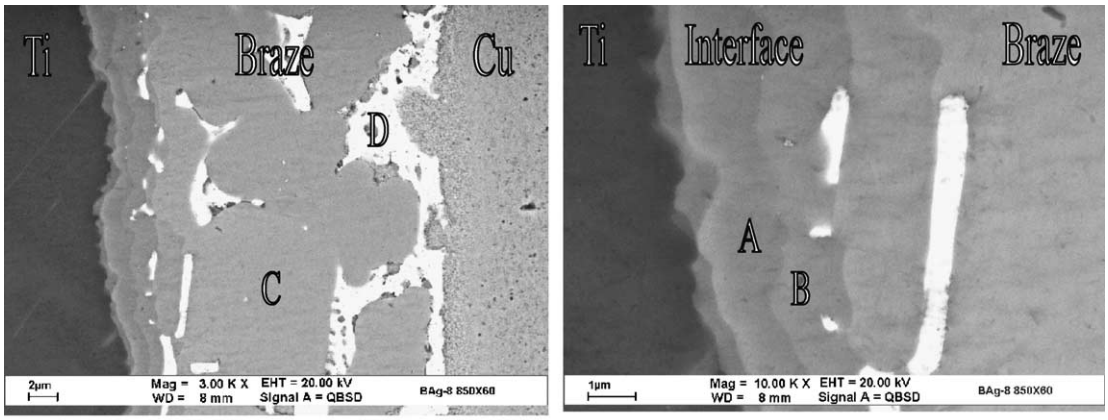

at%	A	B	C	D
Ag	3.2	1.9	2.0	82.7
Cu	46.3	53.5	74.7	16.7
Ti	50.5	44.6	23.3	0.6
Phase	CuTi	Cu_4Ti_3	Cu_4Ti	Ag-rich

Fig. 8. The SEM BEIs and EPMA chemical analysis results of Ti/72Ag–28Cu/Cu specimen infrared brazed at 850 °C for 60 s.

microstructure of the final brazed joint consists of Ag-rich and $TiCu_4$ phases as demonstrated in Fig. 8. In addition to the interfacial Cu_4Ti_3 phase, there is also a CuTi interfacial layer found between the Ti substrate and Cu_4Ti_3 phase.

Fig. 9 shows the SEM BEIs and EPMA chemical analysis results of Ti/72Ag–28Cu/Cu specimen infrared brazed at 800 °C for 60 s. Different from the Fig. 8, the infrared brazed joint is primarily comprised of Cu- and Ag-rich phases as marked by C and D in Fig. 9, respectively. According to Fig. 4, the only invariant reaction below 800 °C is listed below [14]:

$$U_7: \quad L + Cu_4Ti \leftrightarrow Ag + Cu \quad (783\,^{\circ}C) \tag{9}$$

The interfacial reaction between the molten braze and Ti substrate results in forming Cu_4Ti layer. According to Eq. (9), both Ag- and Cu-rich phases are formed upon cooling cycle of the infrared brazing. Consequently, the infrared brazed joint is mainly comprised of Cu- and Ag-rich phases. Fig. 10 displays the isothermal section of Ag–Cu–Ti ternary alloy phase diagram in atomic percent at 700 °C [14]. The compatibility triangle defines the three solid phases that are in

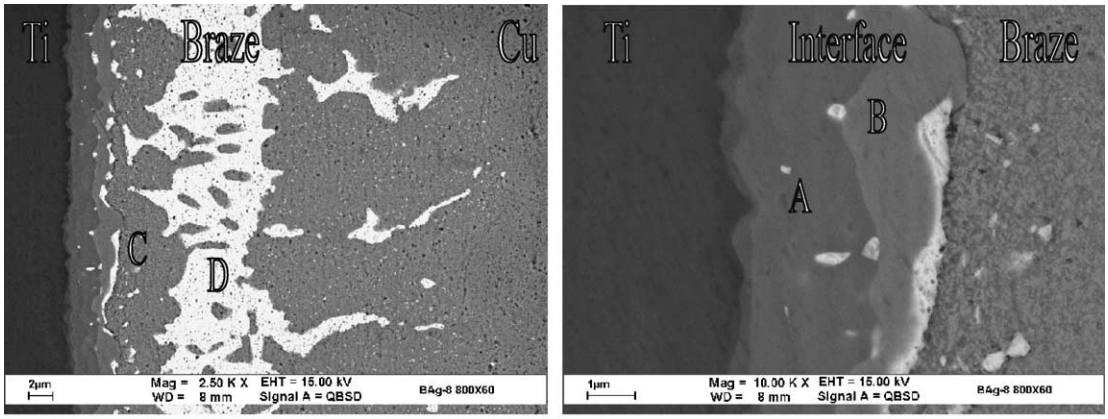

at%	A	B	C	D
Ag	1.9	1.1	4.6	79.4
Cu	54.9	75.1	90.4	19.2
Ti	43.2	23.8	5.1	1.4
Phase	Cu_4Ti_3	Cu_4Ti	Cu-rich	Ag-rich

Fig. 9. The SEM BEIs and EPMA chemical analysis results of Ti/72Ag–28Cu/Cu specimen infrared brazed at 800 °C for 60 s.

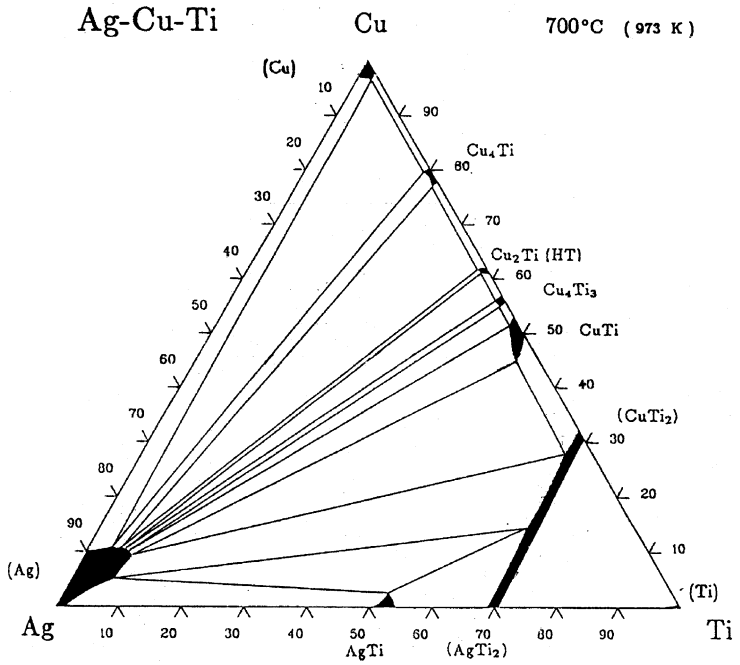

Fig. 10. The isothermal section of Ag–Cu–Ti ternary alloy phase diagram in atomic percent at 700 °C [14].

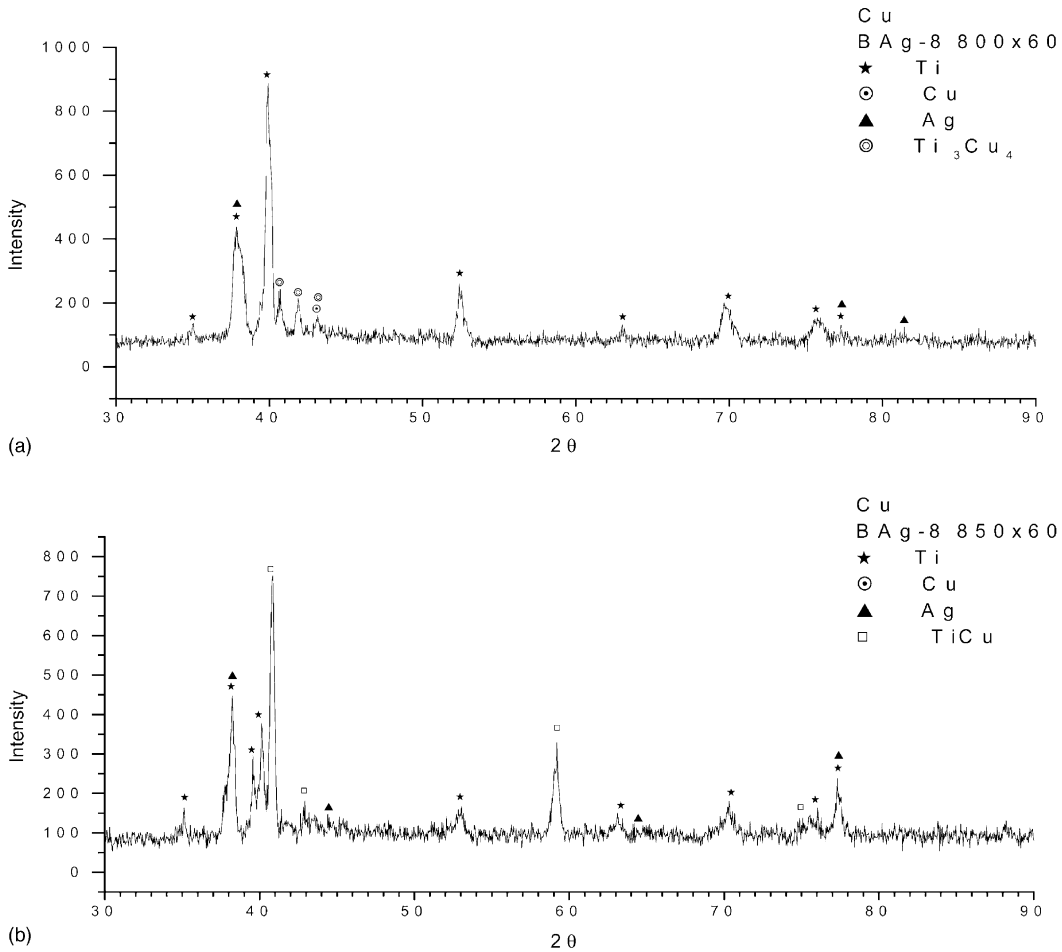

Fig. 11. X-ray structural analyses of the fractured surfaces after shear test for specimens infrared brazed at (a) 800 °C × 60 s and (b) 850 °C × 60 s.

Table 3
The shear strength of infrared brazed Cu/72Ag–28Cu/Ti specimens

Brazing temperature (°C)	Brazing time (s)	Shear strength (MPa)	Average shear strength (MPa)
800	30	13.1	19.4
	30	25.8	
800	60	208.7	209.7
	60	210.7	
850	30	176.4	177.6
	30	178.8	
850	60	82.3	89.7
	60	97.0	

equilibrium after cooling below the solidus temperature [16]. A compatibility triangle consists of Ag, Cu and Cu_4Ti as demonstrated in Fig. 10, and it is in accordance with the microstructural observation of the specimen infrared brazed at 800 °C for 60 s.

Table 3 shows the shear strength of infrared brazed Cu/72Ag–28Cu/Ti specimens. The specimen infrared brazed at 800 °C for 30 s demonstrates low shear strength due to insufficient melting of the braze. There are voids observed at the interface between the Ti substrate and braze. The specimen infrared brazed at 800 °C for 60 s has the highest shear strength among all specimens. Further increasing brazing temperature and/or brazing time deteriorate the shear strength of the joint.

The fractured surface after shear test was further examined by the X-ray analysis. Fig. 11(a) and (b) displays the X-ray structural analyses of the fractured surfaces for specimens infrared brazed at 800 °C × 60 s and 850 °C × 60 s, respectively. Based on the X-ray analyses, the Cu_4Ti_3 phase was observed at the fractured surface of the specimen infrared brazed at 800 °C for 60 s. In contrast, the CuTi phase was found at the fractured surface of the specimen infrared brazed at 850 °C for 60 s. It indicates that the interfacial layer between Ti and the braze alloy plays a crucial role in bonding strength of the joint. The existence of CuTi phase strongly deteriorates the bonding strength of the infrared brazed Cu/72Ag–28Cu/Ti joint, and its shear strength is as low as 89.7 MPa. Fig. 12 displays the SEM fractographs and EDS analyses of infrared brazed specimens after the shear test. Cleavage dominated fractured surfaces are observed for both specimens. Consequently, the formation of interfacial Cu-Ti reaction layer(s) is usually detrimental to the bonding

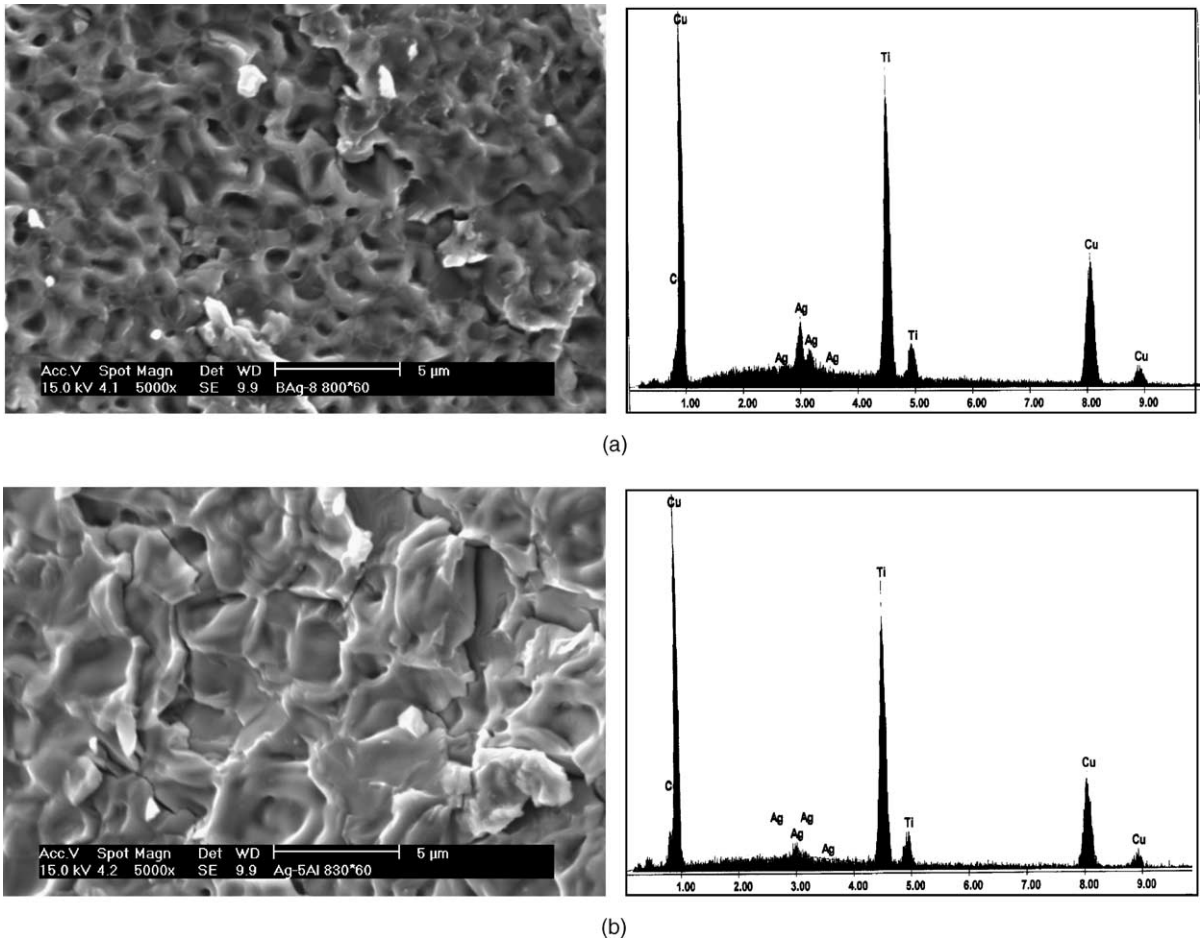

Fig. 12. The SEM fractographs and EDS analyses of infrared brazed specimens after shear test: (a) 800 °C × 60 s and (b) 850 °C × 60 s.

strength of the joint. It is also deduced that the bonding strength of infrared brazed Cu/72Ag–28Cu/Ti joint is strongly related to types of the interfacial reaction layer(s).

4. Conclusions

The microstructural evolution and shear strength of the infrared brazed Ti and Cu with two silver-based braze alloys were extensively evaluated in this study. Important conclusions are summarized below:

1. For the specimen infrared brazed with pure Ag, both Ti and Cu substrates are dissolved into the molten braze during infrared brazing, and the dissolution of substrates into the molten braze results in the chemical composition of the braze alloy deviating from pure silver. The molten braze tends to separate into two liquids, one is rich in Ag, and the other is rich in Cu and Ti.
2. The Ag-rich liquid overflows out of the joint, so only the liquid rich in Ti and Cu is left in the joint. The joint is primarily comprised of Cu_4Ti and Cu_2Ti phases after infrared brazing. Additionally, there are three interfacial reaction layers, including: $CuTi_2$, CuTi and Cu_4Ti_3, respectively. The shear test of infrared brazed Ti/Ag/Cu joint cannot be performed completely due to erosion of the copper substrates.
3. The microstructural evolution of infrared brazed Ti/72Ag–28Cu/Cu joint is in accordance with the Ag–Cu–Ti ternary alloy phase diagram. The interfacial reaction layers between Ti and the braze alloy plays a crucial role in bonding strength of the joint. The Ti/72Ag–28Cu/Cu joint infrared brazed at 800 °C for 60 s demonstrates the highest shear strength up to 209.7 MPa. Further increasing brazing temperature and/or brazing time deteriorate the shear strength of the joint. Cleavage dominated fractured surfaces are observed for specimens infrared brazed at 800 °C and 850 °C for 60 s. Additionally, the formation of interfacial Cu–Ti reaction layer(s) is usually detrimental to the bonding strength of the joint.

Acknowledgements

The authors gratefully acknowledge the financial support from the National Science Council (NSC), Republic of China, under the Grant NSC 91-2216-E002-038.

References

[1] R.K. Shiue, S.K. Wu, J.M. O, J.Y. Wang, Metall. Mater. Trans. 31A (2000) 2527.
[2] C.L. Ou, R.K. Shiue, J. Mater. Sci. 38 (2003) 2337.
[3] R.K. Shiue, S.K. Wu, S.Y. Chen, Acta Mater. 51 (2003) 1991.
[4] T.Y. Yang, S.K. Wu, R.K. Shiue, Intermetallics 9 (2001) 341.
[5] R.K. Shiue, S.K. Wu, C.M. Hung, Metall. Mater. Trans. 33A (2002) 1765.
[6] G. Humpston, D.M. Jacobson, Principles of Soldering and Brazing, ASM International, Metals Park, 1993.
[7] C.C. Liu, C.L. Ou, R.K. Shiue, J. Mater. Sci. 37 (2002) 2225.
[8] D.L. Olson, T.A. Siewert, S. Liu, G.R. Edwards, ASM Handbook, vol. 6, ASM International, Metals Park, 1993.
[9] M. Schwartz, Brazing: For the Engineering Technologist, Chapman & Hall, New York, 1995.
[10] N.A. Dececco, J.N. Parks, Welding J. 32 (1953) 1071.
[11] R.K. Shiue, S.K. Wu, S.Y. Cheng, in: C.T. Liu Symposium on Intermetallic and Advanced Metallic Materials, 2003 TMS Annual Meeting, San Diego, California, USA, 2–6 March 2003.
[12] H.Y. Chan, R.K. Shiue, J. Mater. Sci. Lett. 22 (2003) 1659.
[13] R.E. Lee, Scanning Electron Microscopy and X-ray Microanalysis, Prentice-Hall, New York, 1993.
[14] P. Villars, A. Prince, H. Okamoto, Handbook of Ternary Alloy Phase Diagrams, ASM International, Metals Park, 1995.
[15] T.B. Massalski, Binary Alloy Phase Diagrams, ASM International, Metals Park, 1990.
[16] Y.M. Chiang, D.P. Birnie III, W.D. Kingery, Physical Ceramics, Wiley, New York, 1997.